



Cite this: *RSC Adv.*, 2018, 8, 39074

# Thermally-healable network solids of sulfur-crosslinked poly(4-allyloxystyrene)<sup>†</sup>

Timmy Thiounn,<sup>a</sup> Moira K. Lauer,<sup>a</sup> Monte S. Bedford,<sup>b</sup> Rhett C. Smith <sup>\*a</sup> and Andrew G. Tennyson<sup>\*ab</sup>

Network polymers of sulfur and poly(4-allyloxystyrene), PAOS<sub>x</sub> (*x* = percent by mass sulfur, where *x* is varied from 10–99), were prepared by reaction between poly(4-allyloxystyrene) with thermal homolytic ring-opened S<sub>8</sub> in a thiol-ene-type reaction. The extent to which sulfur content and crosslinking influence thermal/mechanical properties was assessed. Network materials having sulfur content below 50% were found to be thermosets, whereas those having >90% sulfur content are thermally healable and remeltable. DSC analysis revealed that low sulfur-content materials exhibited neither a *T<sub>g</sub>* nor a *T<sub>m</sub>* from –50 to 140 °C, whereas higher sulfur content materials featured *T<sub>g</sub>* or *T<sub>m</sub>* values that scale with the amount of sulfur. DSC data also revealed that sulfur-rich domains of PAOS<sub>90</sub> are comprised of sulfur-crosslinked organic polymers and amorphous sulfur, whereas, sulfur-rich domains in PAOS<sub>99</sub> are comprised largely of α-sulfur (orthorhombic sulfur). These conclusions are further corroborated by CS<sub>2</sub>-extraction and analysis of extractable/non-extractable fractions. Calculations based on TGA, FT-IR, H<sub>2</sub>S trapping experiments, CS<sub>2</sub>-extractable mass, and elemental combustion microanalysis data were used to assess the relative percentages of free and crosslinked sulfur and average number of S atoms per crosslink. Dynamic mechanical analyses indicate high storage moduli for PAOS<sub>90</sub> and PAOS<sub>99</sub> (on the order of 3 and 6 GPa at –37 °C, respectively), with a mechanical *T<sub>g</sub>* between –17 °C and 5 °C. A PAOS<sub>99</sub> sample retains its full initial mechanical strength after at least 12 pulverization-thermal healing cycles, making it a candidate for facile repair and recyclability.

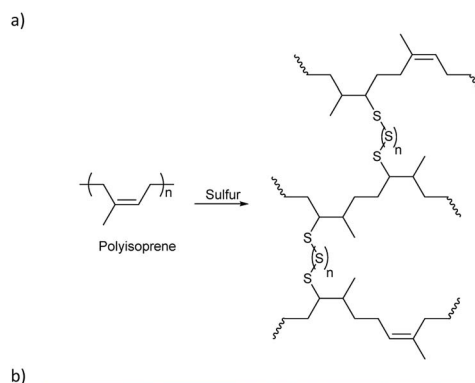
Received 16th August 2018  
 Accepted 12th November 2018

DOI: 10.1039/c8ra06847j

rsc.li/rsc-advances

## Introduction

Vulcanization is a process developed by Charles Goodyear<sup>1</sup> in which the mechanical properties of natural rubber (polyisoprene) are dramatically enhanced by heating it in the presence of up to 5 wt% elemental sulfur (as S<sub>8</sub> at STP). The increase in material strength of a rubber following sulfur vulcanization results from covalent crosslinking between polymer chains.<sup>2</sup> Such crosslinking is derived from homolytic thermal ring opening of S<sub>8</sub> to afford sulfur-centered radicals<sup>3</sup> that subsequently add to C=C bonds, leading to polysulfide crosslinks between polymer chains (Scheme 1a). Without the dramatic increase in mechanical strength endowed upon rubber products by polysulfide crosslinks formed during vulcanization, the modern automobile tire would not be accessible, and early automobiles



**Scheme 1** (a) Sulfur vulcanization of polyisoprene. (b) By-product sulfur at North Vancouver Sulphur Works, originating from tar sand-processing facilities in Alberta, Canada.

<sup>a</sup>Department of Chemistry and Center for Optical Materials Science and Engineering Technologies (COMSET), Clemson University, Clemson, South Carolina, 29634, USA. E-mail: rhett@clemson.edu

<sup>b</sup>Department of Materials Science and Engineering, Clemson University, Clemson, South Carolina, 29634, USA

<sup>†</sup> Electronic supplementary information (ESI) available: Proton NMR of PVP and PAO; IR spectra of PAOS<sub>10–99</sub>; DSC curves of PVP, S<sub>8</sub>, PAO, and PAOS<sub>10–99</sub>. See DOI: 10.1039/c8ra06847j



would have been severely limited in the types and duration of tasks they could perform.

Despite the dramatic structural improvement mediated by sulfur as a minor component by mass of vulcanized rubber, elemental sulfur is currently underutilized as a bulk component of materials. The underutilization of sulfur is especially surprising considering the titanic quantities of S<sub>8</sub> (Scheme 1b) that are produced by petrochemical industries. Petrochemical by-product sulfur is produced by the Claus process,<sup>4,5</sup> wherein H<sub>2</sub>S is oxidized to S<sub>8</sub>. Sulfur removal from fuels is necessary to prevent catalyst poisoning in subsequent steps of the petroleum-refining process and to attenuate the environmental impact of acid rain that results from combustion of sulfur-rich fossil fuels.<sup>6</sup> Currently, the primary use of the S<sub>8</sub> generated from fossil fuels is in the production of sulfuric acid, with lesser quantities being used in fertilizers/pesticides, vulcanization of rubber, and as an additive to asphalt.<sup>7–9</sup> Even after consumption of S<sub>8</sub> by these processes, however, 7 million tons of S<sub>8</sub> accumulate each year as unused waste.<sup>10</sup> Vast quantities of S<sub>8</sub> have been stockpiled at industrial centers and storage sites, so S<sub>8</sub> is an inexpensive, abundant, and readily accessible feedstock for valorization.<sup>6,11–13</sup> Furthermore, the formation of S–S bonds is thermally reversible, a property that could be exploited to generate recyclable thermoplastics and thermally self-healing materials.<sup>14</sup>

Although elemental sulfur itself has very poor mechanical properties, significant advances have been achieved with the advent of inverse vulcanization.<sup>15</sup> Inverse vulcanization is a term coined by Pyun for a process in which S<sub>8</sub> is the bulk material and organic small molecules form the covalent crosslinks between polysulfide chains.<sup>6,15–27</sup> Pyun's breakthrough studies on such high sulfur-content materials have inspired a flurry of related studies to better employ byproduct sulfur.<sup>12</sup> Materials prepared by inverse vulcanization can retain some of the advantageous properties of S<sub>8</sub>. For example, S<sub>8</sub> exhibits high electrical resistivity ( $2 \times 10^{23} \mu\Omega \text{ cm}$ ) and low thermal conductivity ( $0.205 \text{ W m}^{-1} \text{ K}^{-1}$ ). In addition, S<sub>8</sub> actively resists several material degradation pathways, as it is resistant to corrosion by strong acids. It also repels insects and rodents,<sup>28</sup> as well as having antibacterial and anti-microbial properties,<sup>29–34</sup> and has long been used as a treatment for timbers to prevent decay.<sup>35,36</sup> Moreover, if an organic small molecule used in inverse vulcanization has more than one C=C bond, then that molecule can crosslink multiple polysulfide chains to afford a networked covalent composite (NCC) or polymer material.

Many of the inverse vulcanized materials prepared by Pyun exhibit significantly greater durability compared to sulfur itself, even for materials containing >90% sulfur by weight. Because even small amounts of an alkene-functionalized organic small molecule can afford materials with dramatically enhanced mechanical properties relative to pure S<sub>8</sub>, we envisioned that using an alkene-functionalized organic polymer would afford an NCC with enhanced networking. We hypothesized that using this strategy to increase networking in NCCs would increase the mechanical strength of the NCCs. Herein we report the synthesis of allyloxy-functionalized polystyrene, its crosslinking with S<sub>8</sub> *via* inverse vulcanization, and the thermomechanical

properties of the resulting NCCs, PAOS<sub>x</sub> ( $x$  = percent by mass sulfur in the material), wherein  $x$  is varied from 10 to 99.

## Experimental section

### General considerations

All NMR spectra were recorded on a Bruker Avance spectrometer operating at 300 MHz for protons. Thermogravimetric analysis (TGA) was recorded on a TA SDT Q600 instrument over the range 20 to 800 °C, with a heating rate of 5 °C min<sup>-1</sup> under a flow of N<sub>2</sub> (100 mL min<sup>-1</sup>). Differential Scanning Calorimetry (DSC) was acquired using a Mettler Toledo DSC 3 STAR<sup>e</sup> System over the range of -50 to 140 °C, with a heating rate of 10 °C min<sup>-1</sup> under a flow of N<sub>2</sub> (200 mL min<sup>-1</sup>). Each DSC measurement was carried out over five heat-cool cycles to confirm consistent results following the first heat-cool cycle. The data reported were taken from the second cycle of the experiment. Dynamic Mechanical Analysis (DMA) was performed using a Mettler Toledo DMA 1 STAR<sup>e</sup> System in dual cantilever mode. DMA samples were cast from silicone resin molds (Smooth-On Oomoo® 30 tin-cure). The sample dimensions were 1.5 × 8 × 50 mm. Clamping force was 1 cN m and the temperature was varied from -60 to 88 °C with a heating rate of 2 °C min<sup>-1</sup>. The measurement mode was set to displacement control with a displacement amplitude of 5 μm and a frequency of 1 Hz. Fourier transform infrared spectra were obtained using a Shimadzu IRAffinity-1S instrument operating over the range of 400–4000 cm<sup>-1</sup> at ambient temperature using an ATR attachment. Poly(4-vinylphenol) ( $M_w = 11\,000 \text{ g mol}^{-1}$ , Sigma Aldrich), allyl bromide (Oakwood Chemical), elemental sulfur (99.5+%, Duda Energy, LLC) were used without further purification.

### Preparation of poly(4-allyloxystyrene) (PAO)

The procedure that follows is based on a reported method.<sup>37</sup> To a 500 mL round bottom flask equipped with a Teflon-coated magnetic stir bar was added 22.489 g (185.87 mmol) of allyl bromide, 20.000 g (166.44 mmol) of poly(4-vinylphenol) (**PVP**) and 200 mL of acetonitrile. The contents of the flask were stirred for 5 min to facilitate complete dissolution of **PVP**. The flask was then equipped with a water-cooled reflux condenser and placed under an atmosphere of N<sub>2</sub>. The flask was heated in an oil bath at 80 °C while stirring. While the heated reaction mixture was stirring, 49.999 g (361.77 mmol) of K<sub>2</sub>CO<sub>3</sub> was added portionwise to the reaction mixture. The reaction was then refluxed with stirring for 72 h, after which time the mixture was allowed to cool to room temperature. The flask was opened to the air and deionized water (250 mL) was added to the reaction flask to dissolve the remaining K<sub>2</sub>CO<sub>3</sub>.

The reaction mixture was then extracted with dichloromethane (450 mL). The organic layer was collected and washed with 1 M HCl(aq.) (1 × 250 mL), and then with deionized water (1 × 250 mL). The organic layer was collected, and the solvent was evaporated under reduced pressure. The product was collected as a beige solid. <sup>1</sup>H NMR (300 MHz, DMSO-d<sub>6</sub>, δ: 1.41 (br, 2H), 1.72 (br, 1H), 4.45 (br, 2H), 5.21 (br, 1H), 5.35 (br, 1H), 5.99 (br, 1H), 6.48–6.69 (br, 4H). Elemental analysis calculated



for  $C_{11}H_{12}O$ : C, 82.45; H, 7.56%. Found C, 81.88; H, 7.77%. These data are consistent with those previously reported.<sup>37</sup> DSC data for this compound are provided in the ESI.†

### General synthesis of PAOS<sub>x</sub>

Elemental sulfur was weighed directly into an aluminum reaction vessel. The vessel was heated to 180 °C, over which time the sulfur melted. Once the sulfur turned a viscous dark red-orange color (indicative of thermal ring-opening), the appropriate amount of PAO was slowly added to the molten sulfur. The reaction media was manually stirred with a spatula for 60 min. After 60 min the reaction was stopped, the mixture was allowed to cool, and the solid was removed from the reaction vessel. Reagent masses and results of elemental combustion micro-analysis are provided below.

### Synthesis of PAOS<sub>99</sub>

CAUTION: Heating elemental sulfur with organics can result in the formation of H<sub>2</sub>S gas. H<sub>2</sub>S is toxic, foul-smelling, and corrosive. The general synthesis above was used to synthesize PAOS<sub>99</sub> (99 wt% sulfur) where 9.90 g of elemental sulfur and 0.0994 g of PAO were used in the reaction. Elemental analysis calculated: C, 0.82; S, 99.00; H, 0.07%. Found: C, 1.02; S, 98.21; H, 0.0%.

### Synthesis of PAOS<sub>90</sub>

The general synthesis above was used to synthesize PAOS<sub>90</sub> (90 wt% sulfur) where 9.00 g of elemental sulfur and 0.998 g of PAO were used in the reaction. Elemental analysis calculated: C, 8.29; S, 90.00; H, 0.69%. Found: C, 8.07; S, 89.37; H, 0.64%.

### Synthesis of PAOS<sub>80</sub>

The general synthesis above was used to synthesize PAOS<sub>80</sub> (80 wt% sulfur) where 2.40 g of elemental sulfur and 0.600 g of PAO were used in the reaction. Elemental analysis calculated: C, 16.59; S, 80.00; H, 1.40%. Found: C, 16.32; S, 79.70; H, 1.48%.

### Synthesis of PAOS<sub>70</sub>

The general synthesis above was used to synthesize PAOS<sub>70</sub> (70 wt% sulfur) where 2.10 g of elemental sulfur and 0.900 g of PAO were used in the reaction. Elemental analysis calculated: C, 24.89; S, 70.00; H, 2.08%. Found: C, 25.75; S, 63.18; H, 2.24%.

### Synthesis of PAOS<sub>60</sub>

The general synthesis above was used to synthesize PAOS<sub>60</sub> (60 wt% sulfur) where 1.80 g of elemental sulfur and 1.20 g of PAO were used in the reaction. Elemental analysis calculated: C, 33.19; S, 60.00; H, 2.79%. Found: C, 34.54; S, 61.91; H, 3.08%.

### Synthesis of PAOS<sub>50</sub>

The general synthesis above was used to synthesize PAOS<sub>50</sub> (50 wt% sulfur) where 1.50 g of elemental sulfur and 1.50 g of PAO were used in the reaction. Elemental analysis calculated: C, 41.49; S, 50.00; H, 3.49%. Found: C, 41.50; S, 49.90; H, 3.75%.

### Synthesis of PAOS<sub>40</sub>

The general synthesis above was used to synthesize PAOS<sub>40</sub> (40 wt% sulfur) where 1.20 g of elemental sulfur and 1.80 g of PAO were used in the reaction. Elemental analysis calculated: C, 49.78; S, 40.00; H, 4.18%. Found: C, 51.42; S, 37.65; H, 4.81%.

### Synthesis of PAOS<sub>30</sub>

The general synthesis above was used to synthesize PAOS<sub>30</sub> (30 wt% sulfur) where 0.900 g of elemental sulfur and 2.10 g of PAO were used in the reaction. Elemental analysis calculated: C, 58.08; S, 30.00; H, 4.89%. Found: C, 60.25; S, 27.08; H, 5.70%.

### Synthesis of PAOS<sub>20</sub>

The general synthesis above was used to synthesize PAOS<sub>20</sub> (20 wt% sulfur) where 0.600 g of elemental sulfur and 2.40 g of PAO were used in the reaction. Elemental analysis calculated: C, 66.38; S, 20.00; H, 5.58%. Found: C, 66.55; S, 18.22; H, 6.11%.

### Synthesis of PAOS<sub>10</sub>

The general synthesis above was used to synthesize PAOS<sub>10</sub> (10 wt% sulfur) where 0.300 g of elemental sulfur and 2.70 g of PAO were used in the reaction. Elemental analysis calculated: C, 74.67; S, 10.00; H, 6.28%. Found: C, 73.62; S, 9.40; H, 7.10%.

## Results and discussion

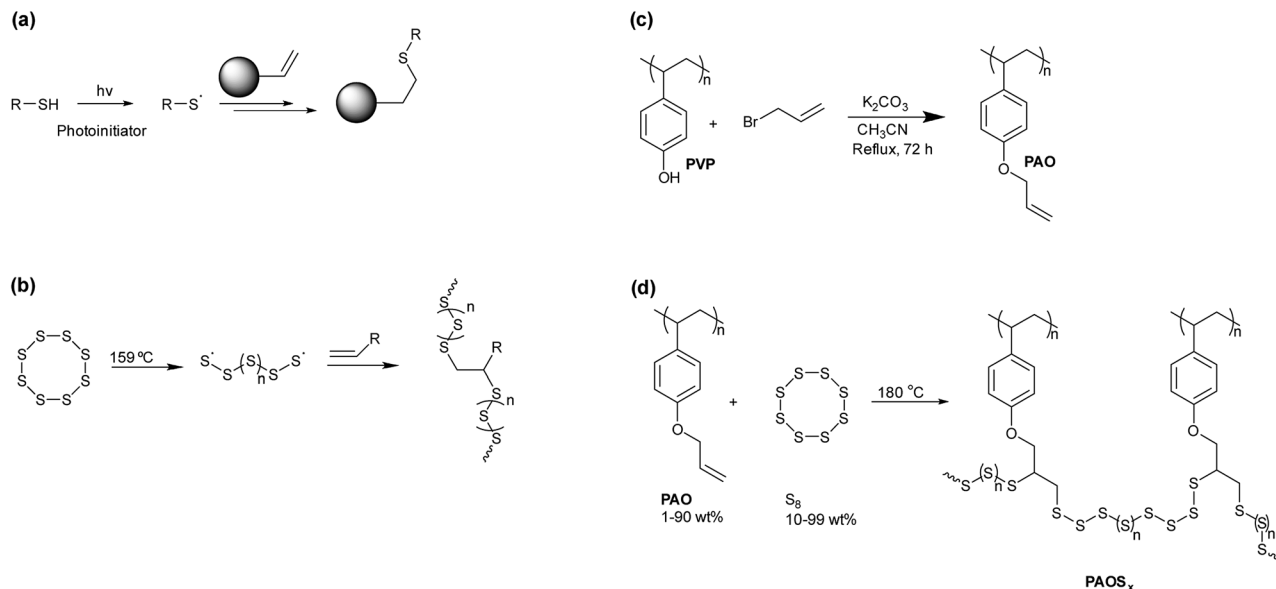
### Synthesis

Polystyrene (PS) was selected as the scaffold for the alkene-bearing polymer substrate to access NCCs because a wide variety of functionalized PS derivatives are commercially available with relatively high molecular weights and well-defined polydispersities. The cross-linking mechanism in inverse vulcanization is analogous to the well-known thiol-ene click reaction (Scheme 2a).<sup>38</sup> Whereas the thiol-ene reaction requires a thiol group and an organic radical initiator to generate a sulfur-centered radical, in inverse vulcanization elemental sulfur (S<sub>8</sub>) undergoes thermal homolytic ring-opening above 159 °C to generate a S-centered radical that can react with an olefin (Scheme 2b).

We reasoned that a PS derivative functionalized with hydroxyl groups could be readily modified with allyl bromide, thus poly(4-vinylphenol) (PVP) was employed as the initial starting material. Exhaustive alkylation was achieved upon reaction of PVP with allyl bromide in the presence of K<sub>2</sub>CO<sub>3</sub>, affording the desired PS derivative with alkene side chains, poly(4-allyloxystyrene) (PAO), in quantitative yield (Scheme 2c).<sup>37</sup>

Analysis of PAO by <sup>1</sup>H NMR and FT-IR spectroscopy (Fig. 1a) revealed that the signals for the OH proton and the O-H stretching vibration (3300 cm<sup>-1</sup>) had disappeared. Two new peaks appeared in the FT-IR spectrum at 922 and 995 cm<sup>-1</sup> that were consistent with monosubstituted alkene (*i.e.*, R-CH=CH<sub>2</sub>) C-H bending modes (Fig. 1b). The ratio of integrals for the allyloxy proton signals to the integral of all PS-backbone proton





Scheme 2 (a) The general synthetic scheme of a thiol–ene reaction. (b) The homolytic ring-opening of  $S_8$  to form a sulfur-centered radical, which then can react with olefins. (c) Synthetic route to prepare PAO. (d) Synthetic route to  $PAOS_x$ , where  $x$  represents the wt% of  $S_8$ .

signals revealed that allylation of hydroxyl groups in **PVP** was quantitative.<sup>39,40</sup>

Thermal reaction of **PAO** with sulfur (Scheme 2d) was achieved by heating the polymer to 180 °C in the presence of varying amounts of sulfur to afford the desired NCCs comprising **PAO** crosslinked with varying relative wt% of sulfur

(**PAOS<sub>x</sub>**;  $x = 10, 20, 30, 40, 50, 60, 70, 80, 90, 99$  wt% S). Each **PAOS<sub>x</sub>** was a brown-red solid with a glass-like appearance. The general physical appearance was consistent across the series, but the materials became more brittle with decreasing wt% sulfur. Mass losses in the range of 2–7% were observed during the reactions of **PAO** with  $S_8$  (Table 1), which were attributed to

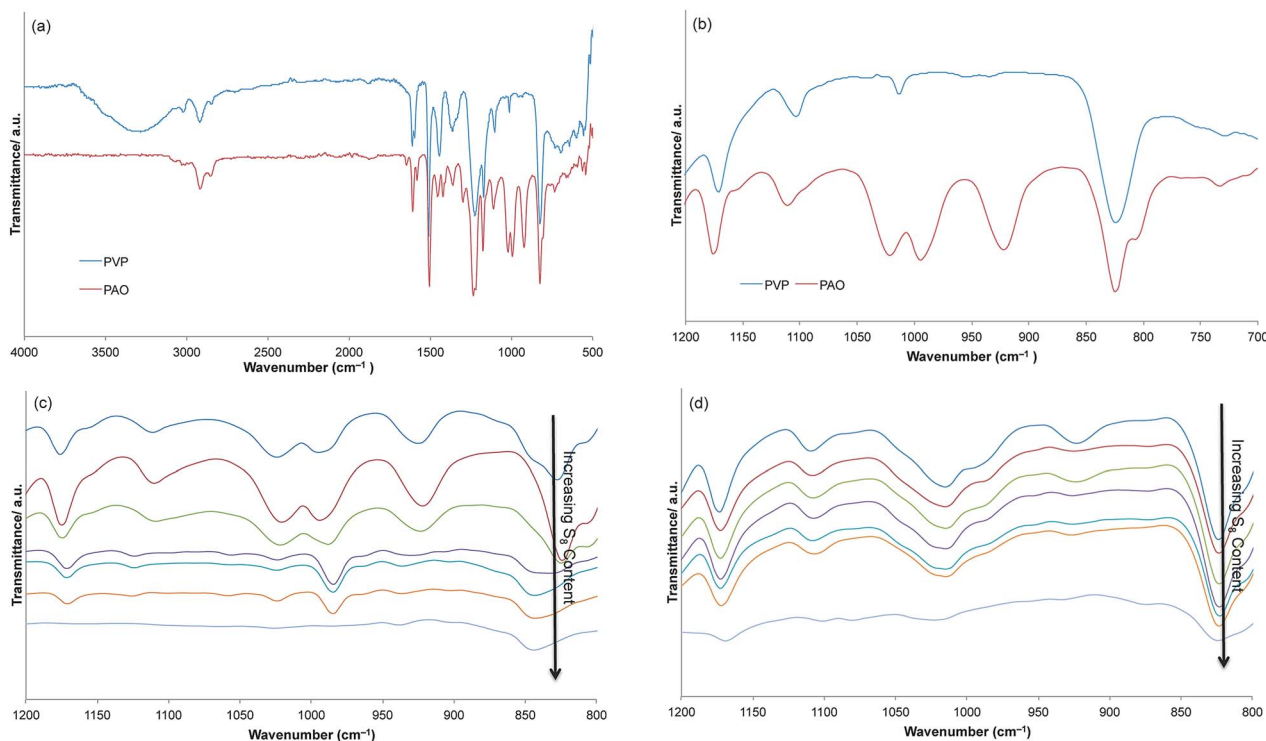


Fig. 1 FT-IR spectra for poly(4-vinylphenol) and PAO over the full scan range (a), poly(4-vinylphenol) and PAO highlighting the range for the monosubstituted alkene C–H bending mode (b),  $CS_2$ -soluble fractions from  $PAOS_x$  ( $x = 40–99$ ), and  $CS_2$ -insoluble fractions from  $PAOS_x$  ( $x = 40–99$ ), (d).



Table 1 Summary of mass loss in synthesis, TGA, and DSC data

Material	$T_d^a$ (°C)	$T_g$ (°C)	$T_m$ (°C)	$T_{\alpha-\beta}$ (°C)	% Mass loss <sup>b</sup> ( $\pm 2\%$ )
PVP	310	— <sup>c</sup>	— <sup>c</sup>	— <sup>c</sup>	NA
PAO	395	43.3	— <sup>c</sup>	— <sup>c</sup>	NA
S <sub>8</sub>	210	— <sup>c</sup>	118.7	— <sup>c</sup>	NA
PAOS <sub>99</sub>	203	— <sup>c</sup>	117.0	— <sup>c</sup>	— <sup>d</sup>
PAOS <sub>90</sub>	191	−37.0	115.8	— <sup>c</sup>	3
PAOS <sub>80</sub>	199	— <sup>c</sup>	116.5	105.3	4
PAOS <sub>70</sub>	192	— <sup>c</sup>	114.3	— <sup>c</sup>	4
PAOS <sub>60</sub>	195	— <sup>c</sup>	114.6	— <sup>c</sup>	3
PAOS <sub>50</sub>	238	— <sup>c</sup>	115.2	103.4	2
PAOS <sub>40</sub>	241	— <sup>c</sup>	116.6	105.8	2
PAOS <sub>30</sub>	244	— <sup>c</sup>	— <sup>c</sup>	— <sup>c</sup>	2
PAOS <sub>20</sub>	263	— <sup>c</sup>	— <sup>c</sup>	— <sup>c</sup>	2
PAOS <sub>10</sub>	290	— <sup>c</sup>	— <sup>c</sup>	— <sup>c</sup>	7

<sup>a</sup>  $T_d$  was determined by calculating the temperature at which 5% mass was lost. <sup>b</sup> Mass loss was determined by weighing the mass of the product after the reaction. <sup>c</sup> No visible transition in the range studied. <sup>d</sup> Was not recorded.

the release of H<sub>2</sub>S gas, as confirmed by elemental microanalysis. CAUTION: H<sub>2</sub>S gas is foul-smelling, toxic, and corrosive and should be trapped as it is produced. Literature examples of H<sub>2</sub>S-trapping strategies include zinc oxide-titanium dioxide sorbents,<sup>41</sup> zinc oxide nanoparticles,<sup>42</sup> reaction with Ag<sup>+</sup> salts for precipitation as Ag<sub>2</sub>S,<sup>43</sup> and other systems.<sup>44</sup> Analysis of PAOS<sub>x</sub> by FT-IR spectroscopy revealed that not all C=C bonds in PAO had reacted with S<sub>8</sub>, as peaks were still observed at 922 and 995 cm<sup>−1</sup> in all samples (spectra are provided in the ESI<sup>†</sup>). Unfortunately, <sup>1</sup>H NMR spectrometric analysis could not be performed due to the poor solubility of PAOS<sub>x</sub> in all solvents examined. Combustion analysis was performed for the elements C, H, N, and S for all PAOS<sub>x</sub>, which demonstrated that S was efficiently incorporated into PAOS<sub>x</sub>.

Given that unreacted C=C linkages remained in each PAOS<sub>x</sub> NCC, we hypothesized that there might also be uncrosslinked S<sub>8</sub>. Each NCC was therefore stirred with an excess of carbon disulfide (CS<sub>2</sub>) to extract and enable quantification of free (non-cross-linked) sulfur. As anticipated, NCCs with higher sulfur contents ( $x > 50$  wt%) comprised substantial amounts of CS<sub>2</sub>-extractable mass. In contrast, PAOS<sub>x</sub> materials containing less than 50 wt% sulfur afforded little to no CS<sub>2</sub>-extractable mass, indicating that essentially all the sulfur is covalently incorporated in these cases. The CS<sub>2</sub>-soluble and insoluble fractions resulting from extraction of PAOS<sub>x</sub> ( $x = 99, 90, 80, 70, 60, 50$ , and 40) were isolated and then analyzed by FT-IR spectroscopy (Fig. 1d). FT-IR analysis suggested that nearly no organics are present in CS<sub>2</sub>-soluble fractions for PAOS<sub>x</sub> ( $x > 50$ ). Elemental analysis on the CS<sub>2</sub>-extractable fraction of PAOS<sub>90</sub> confirmed their identity as being >99% by mass sulfur. The CS<sub>2</sub>-insoluble fraction from PAOS<sub>90</sub> contained 47% by mass of non-extractable sulfur and the FT-IR spectrum confirms nearly complete consumption of the alkene moiety in the polymer backbone. On the basis of the extent of alkene consumption and the amount of non-extractable (crosslinked) sulfur present, the average crosslink is comprised of five sulfur atoms.

## Thermal stability

Thermogravimetric analysis (TGA) of PAOS<sub>x</sub> revealed decomposition temperatures ( $T_d$ , here defined as the temperature at which 5% mass loss was observed upon heating under an atmosphere of N<sub>2</sub>) ranging from 191–290 °C (Fig. 2a). For comparison, the  $T_d$  values for S<sub>8</sub> and PAO are 210 and 395 °C, respectively. For lower sulfur content PAOS<sub>x</sub> ( $x = 10$ –50%),  $T_d$  values generally decreased as the wt% of S<sub>8</sub> increased. However, samples with  $x > 50$  exhibited  $T_d$  values lower than that of S<sub>8</sub> and did not appear to vary significantly in response to changes in S<sub>8</sub> content. This depression of  $T_d$  is attributable to decomposition of an amount of non-crosslinked sulfur corresponding to the amount of CS<sub>2</sub>-extractable sulfur (*vide supra*). Higher sulfur content PAOS<sub>x</sub> ( $x > 70$ ) exhibit very low char yields due to the clean decomposition of sulfur-rich domains, whereas materials containing <70 wt% sulfur – and comprised by

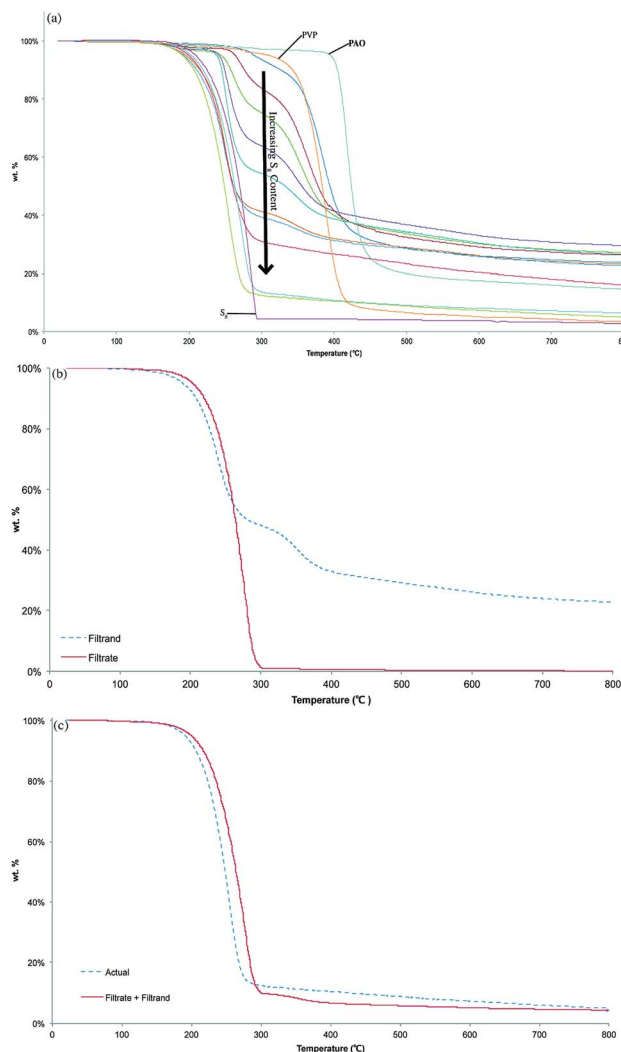


Fig. 2 (a) TGA curves of PVP, PAO, elemental sulfur, and PAOS<sub>x</sub>. (b) The TGA curves for the CS<sub>2</sub>-extractable (solid line) and CS<sub>2</sub>-insoluble fraction (dashed line) of PAOS<sub>90</sub>. (c) The calculated (solid line) TGA curve for independent thermal decomposition of the two fractions overlaid with the experimentally observed TGA curve (dashed line) from the PAOS<sub>90</sub> bulk material.



correspondingly little non-cross-linked sulfur – have char yields ranging from 20–28% (Fig. 2a).

The first degradation step observed for all  $\text{PAOS}_x$  materials was attributed to the loss of the extractable sulfur portion as  $\text{H}_2\text{S}$  gas, which can form *via* hydrodesulfurization reaction between S and the organic components. To confirm this hypothesis, a bulk sample of  $\text{PAOS}_{50}$  was subjected to heating at 250 °C, just above the observed  $T_d$  for this material. The vessel was equipped with a bubbler containing 1 M  $\text{AgNO}_3(\text{aq.})$  to trap evolved  $\text{H}_2\text{S}$  gas *via* reaction with  $\text{AgNO}_3$  to form insoluble  $\text{Ag}_2\text{S}$ . The mass of  $\text{Ag}_2\text{S}$  isolated from this experiment accounts for >83% of the mass loss observed in the TGA trace for  $\text{PAOS}_{50}$ . The shortfall of isolated  $\text{Ag}_2\text{S}$  is likely a result of gas escape prior to reaction or incomplete collection of the finely-dispersed solid.  $\text{PAOS}_x$  samples with  $x < 70$  exhibit a second degradation step at roughly 290 °C attributable to degradation of the organic polymer backbone. The assertion that the covalently-linked and extractable sulfur domains undergo thermal decomposition independently even when commingled in  $\text{PAOS}_{90}$  is further supported by the observation that the curve resulting from summing mass-normalized TGA traces of  $\text{CS}_2$ -soluble and -insoluble fractions is nearly coincident with that of the TGA trace of the original sample of  $\text{PAOS}_{90}$  (Fig. 2C).

### Morphology

Differential scanning calorimetry (DSC) data for fully cured samples of  $\text{PAOS}_x$  are summarized in Table 1.  $\text{PAO}$  is shown to have a  $T_g$  at 43.3 °C, while pure orthorhombic  $\alpha$ -sulfur does not exhibit a glass transition in the range studied. Additionally, sulfur has a melt peak at 118.7 °C. The higher sulfur content  $\text{PAOS}_x$  ( $x = 60$ –99) exhibit endothermic features at  $\sim 106$  °C. The feature at  $\sim 106$  °C in DSC analysis is attributable to an orthorhombic to monoclinic phase change ( $T_{\alpha-\beta}$ , for the  $\alpha\text{-S}(\text{s}) \rightarrow \beta\text{-S}(\text{s})$  process).<sup>45–47</sup> Older literature has variably attributed this transition to occurring at 95 °C,<sup>48–51</sup> possibly confused by the significant variability in properties of sulfur based on its thermal history and complex phase behavior.<sup>36,49,52–55</sup> The peak at  $\sim 115$  °C is attributed to the melt peak of sulfur-rich domains in the materials. The normalized integral of the sulfur melt peak decreases predictably as the wt% of sulfur is decreased (Fig. S13–S24 in the ESI†), consistent with progressively lower amounts of non-cross-linked S in these materials. More interestingly, there is no apparent  $T_g$  in the measured temperature range for any of the  $\text{PAOS}_x$  materials except for  $\text{PAOS}_{90}$ .  $\text{PAOS}_{90}$  exhibits a weakly-observable  $T_g$  at  $-37.0$  °C, a transition which has been suggested in amorphous sulfur as well.<sup>56–58</sup> The lack of a comparable  $T_g$  in even more sulfur-rich  $\text{PAOS}_{99}$  suggests that a lower ratio of cross-linking of  $\text{PAO}$  may facilitate continuity of a more purely orthorhombic sulfur state. An alternate explanation is that  $\text{PAO}$  may act as a plasticizer for amorphous sulfur and stabilize the polymeric and orthorhombic domains in the NCC, consistent with the observed decrease in  $T_g$  for  $\text{PAOS}_{90}$  relative to amorphous sulfur ( $-30$  °C). DSC data show that the lower wt% sulfur materials ( $\text{PAOS}_{10-30}$ ) have neither a  $T_g$  nor a  $T_m$  in the temperature range studied. The predominating

absence of these thermal transitions or those attributable to either orthorhombic sulfur or polymeric sulfur further supports the formulation of  $\text{PAOS}_x$  as extensively cross-linked materials with oligosulfide chains separating organic polymer chains.

### Mechanical properties

One of the primary objectives of the current study was to investigate the extent to which low loading of polymers can endow bulk sulfur with enhanced mechanical strength. On this basis,  $\text{PAOS}_{90}$  and  $\text{PAOS}_{99}$  were selected for study by dynamic mechanical analysis (DMA).

The responses of  $\text{PAOS}_{90}$  and  $\text{PAOS}_{99}$  to flexural stress were studied by DMA in dual cantilever mode with a 1 Hz frequency of oscillation from  $-60$  to 88 °C. The thermal history of sulfur has a dramatic impact on its subsequent thermomechanical properties. To assess whether this would hold true of high sulfur-content NCCs, DMA was undertaken 1.5 h (Fig. 3a–c) and 96 h (Fig. 3d–f) of curing at room temperature after initial melt-casting of samples. The TGA and DSC data discussed in the previous sections is for samples that were cured for at least 96 h. One telling metric in assessing the curing process is the  $T_g$ . The  $T_g$  can be elucidated in many different ways from DMA data.<sup>59</sup> In the present case, the  $T_g$  was determined from the onset of storage modulus ( $T_{g,\text{SM}}$ ) or as a local maximum in either loss modulus ( $T_{g,\text{LM}}$ ) or  $\tan \delta$  curves ( $T_{g,\text{tan}}$ ). For samples analysed 1.5 h after preparation, the onset of storage moduli (Fig. 3a) for  $\text{PAOS}_{90}$  and  $\text{PAOS}_{99}$  occur at the same temperature ( $-17$  °C), however the magnitude of the storage modulus for  $\text{PAOS}_{90}$  is only 50% that of  $\text{PAOS}_{99}$ . The  $T_g$  calculated from loss moduli are  $-4.7$  and  $-6.3$  °C for  $\text{PAOS}_{90}$  and  $\text{PAOS}_{99}$ , respectively. The calculated  $T_g$  from the  $\tan \delta$  peaks are 2.3 °C for  $\text{PAOS}_{90}$  and 5.0 °C for  $\text{PAOS}_{99}$  (Fig. 3c). The magnitude of the  $\tan \delta$  peak provides evidence for effective damping by the material. The damping factor indicates how well a material can dissipate energy through segmental motions or relaxations. Fig. 3c shows that over the entire temperature range studied,  $\text{PAOS}_{99}$  has a higher  $\tan \delta$  value than  $\text{PAOS}_{90}$ . This suggests that  $\text{PAOS}_{99}$  exhibits far more viscous than elastic properties relative to  $\text{PAOS}_{90}$ .  $\text{PAOS}_{99}$  is thus able to dissipate energy more efficiently than its  $\text{PAOS}_{90}$  counterpart. Notably, the  $\tan \delta$  curve for  $\text{PAOS}_{99}$  increases from 60 to 88 °C, a result of the large amounts of free sulfur in the material. These insights further support the inference from DSC data that there is a greater predominance of orthorhombic sulfur in  $\text{PAOS}_{99}$  than in  $\text{PAOS}_{90}$ .

The 96 h-cured samples of  $\text{PAOS}_{90}$  and  $\text{PAOS}_{99}$  were subjected to testing by DMA under identical experimental conditions as were the 1.5 h-cured samples. For comparison, a 96 h-cured sample of pure sulfur is too brittle to be clamped in the DMA instrument even at minimum clamping force. The storage and loss moduli and  $\tan \delta$  curves are shown in Fig. 3d–f. All parameters exhibit modest shifts between 1.5 h and 96 h post-casting. In every case the calculated  $T_g$  increased over the 96 h time period. Table 2 summarizes the calculated  $T_g$  values for  $\text{PAOS}_{90}$  and  $\text{PAOS}_{99}$  after 1.5 and 96 h post-casting. In both  $\text{PAOS}_x$  materials, the storage modulus is seen to increase over the 96 h period, whereas, the  $\tan \delta$  values for both  $\text{PAOS}_x$  materials are shown to decrease over the entire temperature range. The increase in



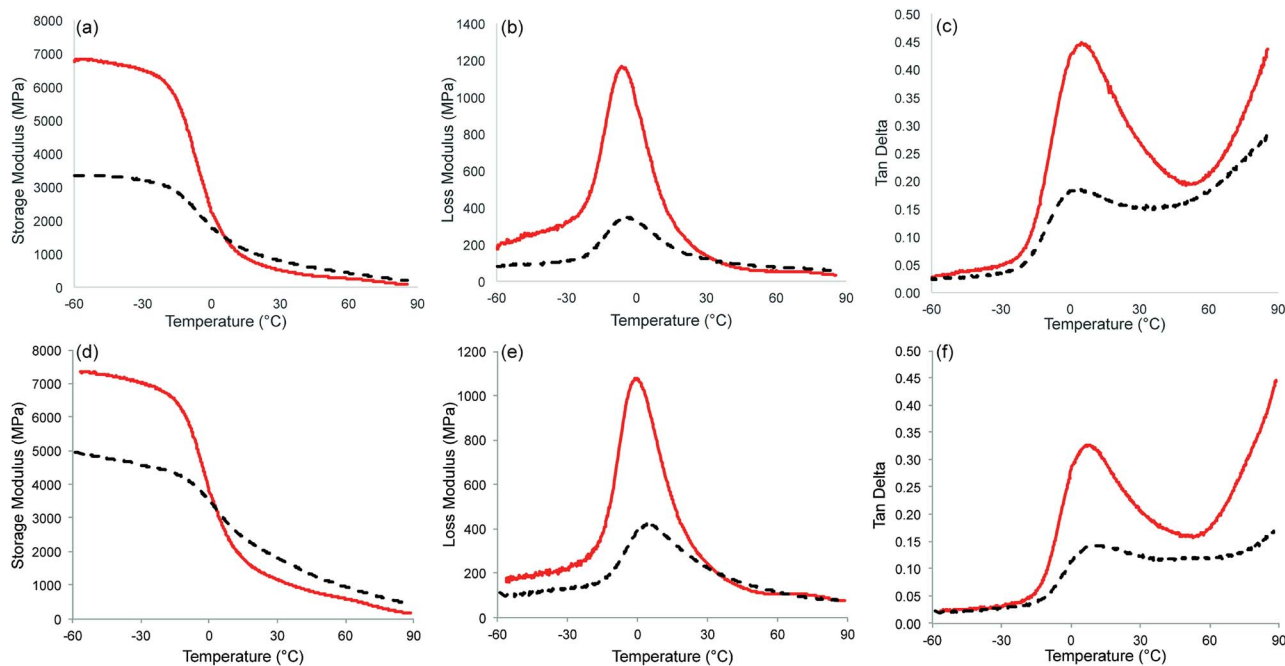


Fig. 3 Temperature dependence of storage and loss modulus and  $\tan \delta$  of PAOS<sub>90</sub> (dashed line) and PAOS<sub>99</sub> (solid line) in dual cantilever mode after 1.5 h of cooling (graphs a–c) and 96 h of cooling (graphs d–f).

Table 2  $T_g$  values for PAOS<sub>90</sub> and PAOS<sub>99</sub> determined from DMA data

Material	$T_{g,SM}$ (°C)		$T_{g,LM}$ (°C)		$T_{g,tan}$ (°C)	
	1.5 h	96 h	1.5 h	96 h	1.5 h	96 h
PAOS <sub>90</sub>	−17	−10	−4.7	5.7	2.3	9.7
PAOS <sub>99</sub>	−17	−13	−6.3	−0.5	5.0	7.3

storage modulus is attributed to the slow reversion of free polymeric sulfur back to the thermodynamically-favored, more crystalline orthorhombic S<sub>8</sub>.<sup>60</sup> Moreover, the decrease in magnitude of  $\tan \delta$  is an indication that the materials' elastic behaviour concomitantly increases.

### Thermal healing and materials comparison

One driving force for the current work was that the thermal reversibility of S–S bond formation offers intriguing possibilities for thermal healing and recycling of high sulfur-content materials. To test the thermal healing/recyclability of PAOS<sub>99</sub>, a sample of the material was subject to DMA analysis and then pulverized into small pieces prior to reannealing to heal the material, and finally allowing the sample to cool to room temperature over 15 min. After repeating this pulverization-thermal healing process ten times, the mechanical properties of the twelve-times-healed sample were identical to that of the first sample within error of the measurement (Fig. 4).

Another driving force behind this study was to determine whether crosslinking by small amounts of organic material could improve the mechanical integrity of bulk sulfur to levels that make it viable for practical applications: without additives

to stabilize it, polymeric sulfur is unstable, reverting to the S<sub>8</sub> form at STP. Comparison of the mechanical features of polymer-cross-linked high-sulfur content PAOS<sub>90–99</sub> to other small molecule-cross-linked, high-sulfur content materials is also of interest. Pyun's group has prepared 1,3,5-triisopropenylbenzene/sulfur crosslinked materials.<sup>61</sup> The storage modulus of this small molecularly-cross-linked material comprising 30 wt% 1,3,5-triisopropenylbenzene and 70 wt% sulfur was 1 GPa at 30 °C under a shear stress. Polymer-cross-linked PAOS<sub>90</sub> and PAOS<sub>99</sub> exhibit a notably higher storage modulus of approximately 2.6 GPa at 30 °C under a flexural stress despite the significantly higher sulfur content in these NCCs.

Compared to other reversibly-crosslinked/thermally healable polymers, PAOS<sub>99</sub> has a higher flexural storage modulus than for epoxy shape-memory polymers<sup>62</sup> and comparable to that of crosslinked and thermally healable (*via* Diels–Alder reaction) poly(dicyclopentadiene)s.<sup>63</sup> The improved mechanical strength

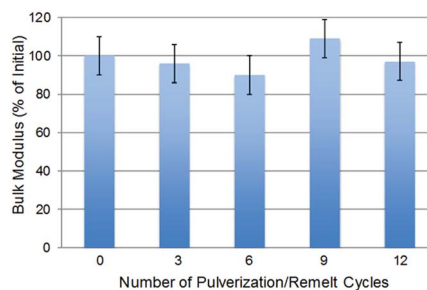


Fig. 4 The bulk modulus (measured at −45 °C) for PAOS<sub>99</sub> after pulverization/remelting cycles remains consistent within error for at least twelve cycles.



of polymer-crosslinked PAOS<sub>x</sub> over other sulfur-rich materials and the similarity in room-temperature storage modulus to polystyrene (1.8 GPa at 30 °C)<sup>64</sup> provide sound proof-of-principle to justify further efforts to prepare value-added materials from affordable/plentiful by-product sulfur by the strategy employed in this study.

## Conclusions

A commercially-available polystyrene derivative was modified to facilitate cross-linking with elemental sulfur. The crosslinked materials, PAOS<sub>x</sub> were prepared with sulfur content of 10–99% by mass. The thermal and mechanical properties of PAOS<sub>x</sub> were elucidated. Target high sulfur-content PAOS<sub>99</sub> and PAOS<sub>90</sub> were comprised of a mixture of sulfur trapped in the amorphous state and short-chain sulfur crosslinks between organic polymer chains. The storage moduli of both PAOS<sub>90</sub> and PAOS<sub>99</sub> increased over a 96 h setting time as free polymeric sulfur slowly relaxed to the orthorhombic state. The fully-set mechanical strength of even PAOS<sub>99</sub>, which is 99% by mass sulfur, increased significantly when compared to a pure sulfur sample prepared under the same conditions. PAOS<sub>99</sub> maintains its mechanical integrity after physical breakdown and thermally recasting for at least a dozen cycles, demonstrating the facile recyclability of these materials. PAOS<sub>90</sub> and PAOS<sub>99</sub> materials thus show promise for valorizing elemental sulfur as a component of durable, recyclable material applications for which petrochemicals are currently used. Follow-up studies on improving the mechanical properties of high sulfur-content network solids are currently underway.

## Conflicts of interest

There are no conflicts to declare.

## Acknowledgements

This work was supported by the National Science Foundation (CHE-1708844). Gratitude is kindly extended for assistance from Tucker McFarlane of Stephen F. Foulger's Group (Clemson University, TGA and DSC). We thank Catherine A. Conrad for help with early work to begin this project.

## Notes and references

- G. Charles, *US Pat.* 3633A, 1844.
- E. H. Farmer and F. W. Shipley, *J. Chem. Soc.*, 1947, 1519–1532, DOI: 10.1039/jr9470001519.
- R. S. Glass, *Top. Curr. Chem.*, 2018, **376**, 1–42.
- X. Zhang, Y. Tang, S. Qu, J. Da and Z. Hao, *ACS Catal.*, 2015, **5**, 1053–1067.
- A. Demirbas, H. Alidrisi and M. A. Balubaid, *Pet. Sci. Technol.*, 2015, **33**, 93–101.
- J. Lim, J. Pyun and K. Char, *Angew. Chem., Int. Ed.*, 2015, **54**, 3249–3258.
- D.-y. Lee, *Ind. Eng. Chem. Prod. Res. Dev.*, 1975, **14**, 171–177.
- Elemental Sulfur and Sulfur-Rich Compounds I, in *Top. Curr. Chem.*, ed. R. Steudel, 2003, 230, p. 2003.
- Elemental Sulfur and Sulfur-Rich Compounds II, in *Top. Curr. Chem.*, ed. R. Steudel, 2003, 231, p. 2003.
- G. Kutney, *Sulfur. History, Technology, Applications & Industry*, ChemTec, Toronto, 2007.
- U. S. G. Survey, *Mineral Commodity Summaries*, 2017, p. 202, DOI: 10.3133/70180197.
- M. J. H. Worthington, R. L. Kucera and J. M. Chalker, *Green Chem.*, 2017, **19**, 2748–2761.
- M. P. Crockett, A. M. Evans, M. J. H. Worthington, I. S. Albuquerque, A. D. Slattery, C. T. Gibson, J. A. Campbell, D. A. Lewis, G. J. L. Bernardes and J. M. Chalker, *Angew. Chem., Int. Ed.*, 2016, **55**, 1714–1718.
- F. Garcia and M. M. J. Smulders, *J. Polym. Sci., Part A: Polym. Chem.*, 2016, **54**, 3551–3577.
- W. J. Chung, J. J. Griebel, E. T. Kim, H. Yoon, A. G. Simmonds, H. J. Ji, P. T. Dirlam, R. S. Glass, J. J. Wie, N. A. Nguyen, B. W. Guralnick, J. Park, A. Somogyi, P. Theato, M. E. Mackay, Y.-E. Sung, K. Char and J. Pyun, *Nat. Chem.*, 2013, **5**, 518–524.
- Y. Zhang, K. M. Konopka, R. S. Glass, K. Char and J. Pyun, *Polym. Chem.*, 2017, **8**, 5167–5173.
- Y. Zhang, J. J. Griebel, P. T. Dirlam, N. A. Nguyen, R. S. Glass, M. E. MacKay, K. Char and J. Pyun, *J. Polym. Sci., Part A: Polym. Chem.*, 2017, **55**, 107–116.
- J. Park, E. T. Kim, C. Kim, J. Pyun, H.-S. Jang, J. Shin, J. W. Choi, K. Char and Y.-E. Sung, *Adv. Energy Mater.*, 2017, **7**, 1700074.
- V. P. Oleshko, A. A. Herzing, C. L. Soles, J. J. Griebel, W. J. Chung, A. G. Simmonds and J. Pyun, *Microsc. Microanal.*, 2016, **22**, 1198–1221.
- V. P. Oleshko, A. A. Herzing, K. A. Twedt, J. J. Griebel, J. J. McClelland, J. Pyun and C. L. Soles, *Langmuir*, 2017, **33**, 9361–9377.
- J. Lim, U. Jung, W. T. Joe, E. T. Kim, J. Pyun and K. Char, *Macromol. Rapid Commun.*, 2015, **36**, 1103–1107.
- E. T. Kim, W. J. Chung, J. Lim, P. Johe, R. S. Glass, J. Pyun and K. Char, *Polym. Chem.*, 2014, **5**, 3617–3623.
- E. T. Kim, J. Park, C. Kim, A. G. Simmonds, Y.-E. Sung, J. Pyun and K. Char, *ACS Macro Lett.*, 2016, **5**, 471–475.
- J. J. Griebel, N. A. Nguyen, A. V. Astashkin, R. S. Glass, M. E. MacKay, K. Char and J. Pyun, *ACS Macro Lett.*, 2014, **3**, 1258–1261.
- J. J. Griebel, N. A. Nguyen, S. Namnabat, L. E. Anderson, R. S. Glass, R. A. Norwood, M. E. MacKay, K. Char and J. Pyun, *ACS Macro Lett.*, 2015, **4**, 862–866.
- J. J. Griebel, G. Li, R. S. Glass, K. Char and J. Pyun, *J. Polym. Sci., Part A: Polym. Chem.*, 2015, **53**, 173–177.
- P. T. Dirlam, A. G. Simmonds, T. S. Kleine, N. A. Nguyen, L. E. Anderson, A. O. Klever, A. Florian, P. J. Costanzo, P. Theato, M. E. Mackay, R. S. Glass, K. Char and J. Pyun, *RSC Adv.*, 2015, **5**, 24718–24722.
- K. J. Rao and S. Paria, *RSC Adv.*, 2013, **3**, 10471–10478.
- U. S. E.P.A., *R.E.D. Sulfur Facts*, U.S. Environmental Protection Agency, Pesticides and Toxic Substances Branch, Washington, D.C., 1991.



- 30 R. Musah, S. Kim and R. Kubec, *Phosphorus, Sulfur Silicon Relat. Elem.*, 2005, **180**, 1455–1456.
- 31 S. Kim, R. Kubec and R. A. Musah, *J. Ethnopharmacol.*, 2006, **104**, 188–192.
- 32 J. T. Weld and A. Gunther, *J. Exp. Med.*, 1947, **85**, 531–542.
- 33 G. B. Lawson, *Am. Rev. Tuberc.*, 1934, **29**, 650–651.
- 34 L. Libenson, F. P. Hadley, A. P. McIlroy, V. M. Wetzel and R. R. Mellon, *J. Infect. Dis.*, 1953, **93**, 28–35.
- 35 G. Robert and S. W. John Jr, Application, WO Pat., 1997-US19812 9818872, 1998.
- 36 M. Takeji, Application, US Pat., 1976-754266 4127686, 1978.
- 37 C. Wang, W.-Y. Lee, R. Nakajima, J. Mei, D. H. Kim and Z. Bao, *Chem. Mater.*, 2013, **25**, 4806–4812.
- 38 A. B. Lowe, *Polym. Chem.*, 2014, **5**, 4820–4870.
- 39 A. V. Raghu, G. S. Gadaginamath, N. Mathew, S. B. Halligudi and T. M. Aminabhavi, *J. Appl. Polym. Sci.*, 2007, **106**, 299–308.
- 40 D. S. Donawade, A. V. Raghu, U. M. Muddapur and G. S. Gadaginamath, *Indian J. Chem., Sect. B: Org. Chem. Incl. Med. Chem.*, 2005, **44B**, 1470–1475.
- 41 S. Lew, K. Jothimurugesan and M. Flytzani-Stephanopoulos, *Ind. Eng. Chem. Res.*, 1989, **28**, 535–541.
- 42 M. A. Sayyadnejad, H. R. Ghaffarian and M. Saeidi, *Int. J. Environ. Sci. Technol.*, 2008, **5**, 565–569.
- 43 M. Arslan, B. Kiskan and Y. Yagci, *Macromolecules*, 2016, **49**, 767–773.
- 44 S. Potivichayanon, P. Pokethitiyook and M. Kruatrachue, *Process Biochem.*, 2006, **41**, 708–715.
- 45 Q. Lian, Y. Li, K. Li, J. Cheng and J. Zhang, *Macromolecules*, 2017, **50**, 803–810.
- 46 S. Z. Khawaja, S. Vijay Kumar, K. K. Jena and S. M. Alhassan, *Mater. Lett.*, 2017, **203**, 58–61.
- 47 V. K. Shankarayya Wadi, K. K. Jena, S. Z. Khawaja, K. Yannakopoulou, M. Fardis, G. Mitrikas, M. Karagianni, G. Papavassiliou and S. M. Alhassan, *ACS Omega*, 2018, **3**, 3330–3339.
- 48 B. Meyer, *Chem. Rev.*, 1964, **64**, 429–451.
- 49 B. Meyer, *Inorg. Sulphur Chem.*, 1968, 241–258.
- 50 B. Meyer, *Adv. Inorg. Chem. Radiochem.*, 1976, **18**, 287–317.
- 51 B. Meyer, *Chem. Rev.*, 1976, **76**, 367–388.
- 52 R. F. Bacon and R. Fanelli, *J. Am. Chem. Soc.*, 1943, **65**, 639–648.
- 53 R. H. Arntson, F. W. Dickson and G. Tunell, *Science*, 1958, **128**, 716–718.
- 54 Y. Akahama, M. Kobayashi and H. Kawamura, *Phys. Rev. B: Condens. Matter Mater. Phys.*, 1993, **48**, 6862–6864.
- 55 A. G. M. Ferreira and L. Q. Lobo, *J. Chem. Thermodyn.*, 2010, **43**, 95–104.
- 56 A. V. Tobolsky, *J. Polym. Sci., Part C: Polym. Symp.*, 1966, **12**, 71–78.
- 57 A. V. Tobolsky, *J. Polym. Sci., Part C: Polym. Symp.*, 1966, **12**, 71–78.
- 58 A. V. Tobolsky, W. MacKnight, R. B. Beevers and V. D. Gupta, *Polymer*, 1963, **4**, 423–427.
- 59 K. Menard, *Dynamic Mechanical Analysis: A Practical Introduction to Techniques and Applications*, CRC, 1999.
- 60 N. L. Batista, P. Olivier, G. Bernhart, M. C. Rezende and E. C. Botelho, *Mater. Res.*, 2016, **19**, 195–201.
- 61 T. S. Kleine, N. A. Nguyen, L. E. Anderson, S. Namnabat, E. A. LaVilla, S. A. Showghi, P. T. Dirlam, C. B. Arrington, M. S. Manchester, J. Schwiegerling, R. S. Glass, K. Char, R. A. Norwood, M. E. Mackay and J. Pyun, *ACS Macro Lett.*, 2016, **5**, 1152–1156.
- 62 J. Hu, W. Chen, P. Fan, J. Gao, G. Fang, Z. Cao and F. Peng, *Polym. Test.*, 2017, **62**, 335–341.
- 63 E. B. Murphy, E. Bolanos, C. Schaffner-Hamann, F. Wudl, S. R. Nutt and M. L. Auad, *Macromolecules*, 2008, **41**, 5203–5209.
- 64 M. Worzakowska, *J. Therm. Anal. Calorim.*, 2015, **121**, 235–243.

